Abstract

Numerous studies have been done on a possible fourth generation of fermions. This work is another examination of the hypothetical fourth generation, with the introduction of an ansatz used in two Higgs doublet model type III. This ansatz makes $T \rightarrow t+H$ the overwhelmingly dominant decay mode for the fourth generation top quark, if kinematically accessible. Provided that the neutral Higgs particle has sufficient mass, this decay mode has virtually no background and yields eight lepton and four lepton events which would both be a clear signature of a fourth generation and the Higgs boson.

1. Introduction

With the advent of new high energy colliders, such as the Large Hadron Collider (LHC) at CERN, the field of high energy particle physics is primed for a change. The Standard Model (SM) of particle physics, despite its tremendous success, fails to answer a number of questions. Why do only a certain number of quarks exist? Why are the masses of these quarks so irregular? Why do these quarks have regular charges? Are there quarks beyond those discovered so far? These shortfalls, among others, have led particle physicists to consider other theories. While Grand Unified Theories (GUTs) are appealing, a modest extension of the SM may be more likely. A fourth generation of fermions is one of the simplest extensions possible.

There are two types of particles in the Standard Model: fermions and bosons. Bosons are particles with integer spin and are responsible for mediating the four known forces. The photon is a massless, chargeless, spin 1 particle which carries the electromagnetic force. The strong force is transmitted by the gluon, also a massless, chargeless particle with spin 1. The weak force is transmitted by three bosons: the W^+, W^-, and Z^0 bosons. The W^+ and W^- are spin 1 particles carrying a charge of +1 and -1 respectively. The Z^0 is a spin 1 chargeless particle. All the bosons transmitting the weak force are heavy particles, with masses on the order of 100 GeV. The boson transmitting the gravitational force is postulated to be the graviton, but has not yet been discovered. The Higgs boson is a long sought particle which is believed to generate the mass of all particles in the universe. Since the Higgs boson has never been observed the exact number of Higgs particles and their masses remains an open question. Numerous theories concerning the structure of the Higgs sector exist.

Fermions are particles with half integer spin that constitute all matter in the universe. The fermion sector is composed of quarks and leptons, divided into three generations. Each generation contains a pair of quarks, one with charge 2/3 (up-like) and one with charge -1/3 (down-like), and a pair of leptons. One lepton is a very light chargeless particle called a neutrino and the other lepton is an electron or similar particle with charge of -1. The first generation contains the up quark, down quark, electron, and electron neutrino. The second generation is composed of the charm quark, strange quark, muon, and muon neutrino. The third generation has the top quark, bottom quark, tau, and tau neutrino. The three generations of quarks and leptons described previously are thought to complete the fermion sector. Indeed, accurate measurements of the Z width in 1989 confirmed that precisely three light neutrinos exist. Therefore, a fourth family of quarks and leptons would necessitate the existence of a heavy neutrino of mass greater than 45 GeV [1].

There are a number of theoretical considerations which make the fourth generation an attractive concept. A fourth family of fermions can lead to unification of the gauge couplings at the unification scale [1]. The strong CP problem can be resolved in a model with two additional generations of quarks [1]. Finally, there is no reason forbidding a fourth generation other than the current inability to achieve the energy required for its observation. The possibility of additional generations cannot be ignored until experiment either confirms or disproves their existence. This project investigates the possibility of a fourth generation interacting with a nonstandard parameterization of the Higgs sector, the two Higgs doublet model (2HDM) type III, at the LHC.

2. Theory

2.1 Electroweak Spontaneous Symmetry Breaking: The Higgs Boson

Gauge theories have been applied to particle physics with great success. For instance, Quantum Electrodynamics (QED) is a gauge theory which has the highest degree of theoretical-experimental agreement ever achieved. However attempts to apply gauge theories to the massive gauge bosons ($W^{\pm}$, Z) proved unsuccessfully initially. Examining the QED Lagrangian demonstrates why [3].

$$L = \overline{\psi}\left(i\gamma^{\mu}\partial_{\mu} - m\right)\psi + e\,\overline{\psi}\gamma^{\mu}A_{\mu}\psi - \frac{1}{4}F_{\mu\nu}F^{\mu\nu} \tag{1}$$

Here ψ is the wavefunction, $\overline{\psi} \equiv \psi^{t}\gamma^{0}$ where ψ^{t} is the hermitian conjugate of ψ, γ^{μ} are the Dirac matrices, $F_{\mu\nu}$ is the field strength tensor, A_{μ} is a vector field dubbed the *gauge field* whose introduction was required as part of demanding local gauge invariance, and finally *e* is the electron charge. Since we are using a gauge theory, we must demand gauge invariance of the Lagrangian under the local gauge transformations $\psi \rightarrow e^{i\alpha}\psi$ and $A_{\mu} \rightarrow A_{\mu} + \frac{1}{e}\partial_{\mu}\alpha$ for arbitrary α. Modifying this Lagrangian via the introduction of the mass term $\frac{1}{2}m^{2}A_{\mu}A^{\mu}$ destroys gauge invariance [3]. Since such a term is forbidden, we are forced to conclude that the gauge particle in QED, the photon, is massless. However the gauge particles of the electroweak (unified electromagnetic and weak) force are the W bosons and Z boson in addition to the photon. These bosons have masses on the order of 100 GeV. Thus any attempt to treat the electroweak force with a gauge theory prescription necessitates the introduction of a mass term into equation 1. Local gauge invariance in the Lagrangian can be preserved through a process called spontaneous

symmetry breaking via the introduction of the Higgs boson. A world consisting of only these neutral Higgs particles can be described with the following Lagrangian [3]:

$$L = \frac{1}{2}(\partial_\mu \varphi)^2 - \left(\frac{1}{2}m^2\varphi^2 + \frac{1}{4}\lambda\varphi^4\right) \quad (2)$$

Here φ is the field generated by the Higgs bosons and λ and m are parameters such that $m^2 < 0$ and $\lambda > 0$. This Lagrangian is invariant under a reflection symmetry operation, $\varphi \rightarrow -\varphi$. If we allow m^2 to be positive, it creates the potential shown in Figure 1a. This potential is minimized by $\varphi = 0$, the Higgs vacuum expectation value. However if m^2 is negative, we find that there are two nonzero Higgs vacuum expectation values which minimize our potential, $\varphi = \pm v$ as shown in Figure 1b. This forces us to make an arbitrary choice as to which value of φ shall be our vacuum expectation value, thereby breaking reflection symmetry invariance. From this vacuum expectation value it can be shown that the gauge particle for this field indeed possesses a mass. This prescription is used to generate the masses of not only the W and Z bosons, but all massive particles in the Standard Model [3].

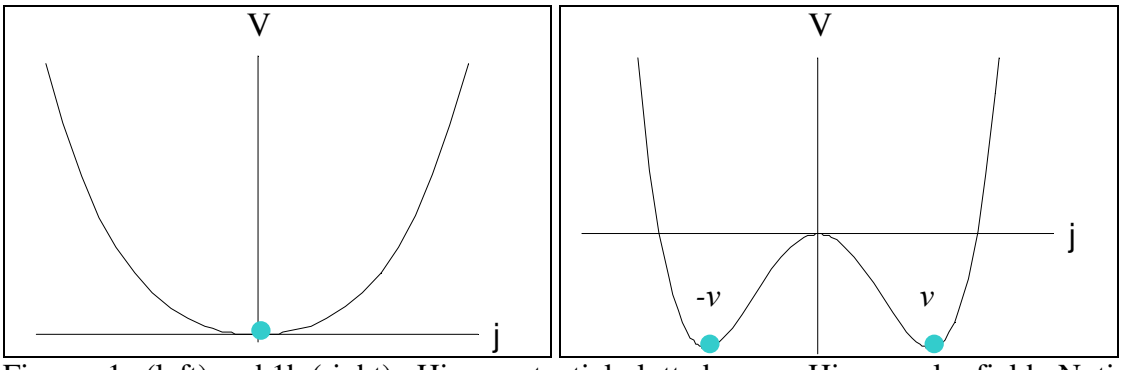

Figures 1a (left) and 1b (right). Higgs potential plotted versus Higgs scalar field. Notice that if $m^2 > 0$ (left) there is one minimum at 0 which is symmetric under transformations. However if $m^2 < 0$ (right) the potential takes a saddle form. With two minimizing points. Choosing one of these values, $\varphi = \pm v$, as *the* minimizing value (vacuum expectation value of the Higgs scalar field) breaks symmetry of the Lagrangian and allows the addition of mass terms.

Experimental determination of the W and Z masses has allowed the determination of the Higgs vacuum expectation value [4]:

$$v = \frac{2M_W}{g} = \left(\sqrt{2}G_F\right)^{-\frac{1}{2}} = 246\,\text{GeV}. \tag{3}$$

Here G_F is Fermi's constant, M_W is the mass of the W boson, and g is the electroweak coupling. The manifestation of particle mass is determined by a particle's coupling to the Higgs field. These couplings are termed the Yukawa couplings and are determined experimentally. The mass for a lepton i takes the form [4]:

$$\begin{aligned} &m_i = G_i v/\sqrt{2}, \\ &i \in \{e, \mu, \tau\}. \end{aligned} \tag{4}$$

G_i is the Yukawa coupling between the lepton and the Higgs field and i may be any of the three known massive leptons. The mass generation for quarks is slightly more complex. The collection of up-like quarks *(u, c, t)* and down-like quarks *(d, s, b)* each has their own three by three mass matrices which couple to the Higgs field via two distinct three by three Yukawa coupling matrices [4]:

$$\begin{aligned} &M^u{}_{ij} = G^u{}_{ij}\, v/\sqrt{2},\ M^d{}_{kl} = G^d{}_{kl}\, v/\sqrt{2}, \\ &(i, j) \in \{u, c, t\},\ (k, l) \in \{d, s, b\}. \end{aligned} \tag{5}$$

Here $M^u{}_{ij}$ and $M^d{}_{kl}$ are the three by three mass matrices for up-like and down-like quarks respectively, and $G^u{}_{ij}$ and $G^d{}_{kl}$ are the three by three Yukawa coupling matrices for up-like and down-like quarks respectively. These mass and coupling matrices may be diagonalized via unitary transformations. Once in diagonal form, elementary quark masses can simply be read off the diagonal. Note that the coupling matrices chosen above are arbitrary, determined by experiment rather than derived. From the above

equations all interactions of the Higgs field with particles are known. Unfortunately the mass of the Higgs particle itself is unknown.

2.2 The Two Higgs Doublet Model

The two Higgs doublet model (2HDM) differs from the SM prescription in that rather than there being one neutral Higgs boson, there are two neutral Higgs bosons *(H^0, h^0)*, a charged pair of Higgs bosons *($H^{\pm}$)*, and a CP-odd scalar particle *(A^0)*. Since there are now two Higgs doublets the matrix equation for up-like quarks becomes:

$$M^{u}{}_{ij} = G^{(1,u)}{}_{ij}\, v_1/\sqrt{2} + G^{(2,u)}{}_{ij}\, v_2/\sqrt{2}, \quad (i,j) \in \{u,c,t\}. \tag{6}$$

A similar modification occurs for the down-like quark matrix. This is an extremely important difference from the SM Higgs. In the standard Higgs model, the presence of only one coupling matrix allows the mass matrix and the coupling matrix to diagonalize simultaneously, thus eliminating the presence of Flavor Changing Neutral Current (FCNC) interactions (such as $\bar{s} \to d + h^0$ interactions). This is not true in the standard 2HDM. The two coupling matrices do not diagonalize simultaneously, which allows the problematic FCNCs to exist. The presence of FCNCs would contradict observations of rare kaon decays which imply that FCNCs are heavily suppressed. In order to create a model with physical implications, these currents must be suppressed by some mechanism. In the 2HDM FCNCs are suppressed by implementing discrete symmetries, referred to as types I and II, or in type III by adopting the popular ansatz in which the FCNC Yukawa couplings are proportional to $\sqrt{m_i m_j}$, where m_i and m_j are particle masses. This ansatz heavily suppresses any FCNCs. However, if a fourth generation exists then the respective

coupling constant with the third generation will be huge, leading to numerous interactions between the two generations [5].

2.3 Calculation of Decay Widths for Fourth Generation Quarks

All calculations were carried out in standard particle physics units and all results are presented in GeV. Here the decay rates for the fourth family quarks, denoted T and B, are computed for the following decay processes: $T\rightarrow(t+Z^0,\ t+h^0,\ B+W^+,\ b+W^+,\ c+W^+)$ for the fourth generation top quark and $B\rightarrow(b+Z^0,\ b+h^0,\ t+\ W^-,\ s+W^-)$ for the fourth generation bottom quark. $W^{\pm}$ may be real or virtual; however Z^0 and h^0 are strictly real particles. $T\rightarrow t+\gamma$ is similar to $T\rightarrow t+Z^0$ but less significant and thus not considered here. The lightest type III Higgs boson, h^0, will be referred to as H from this point on since it is the only Higgs particle considered in our calculations. The relevant Feynman diagrams are shown in Figure 2:

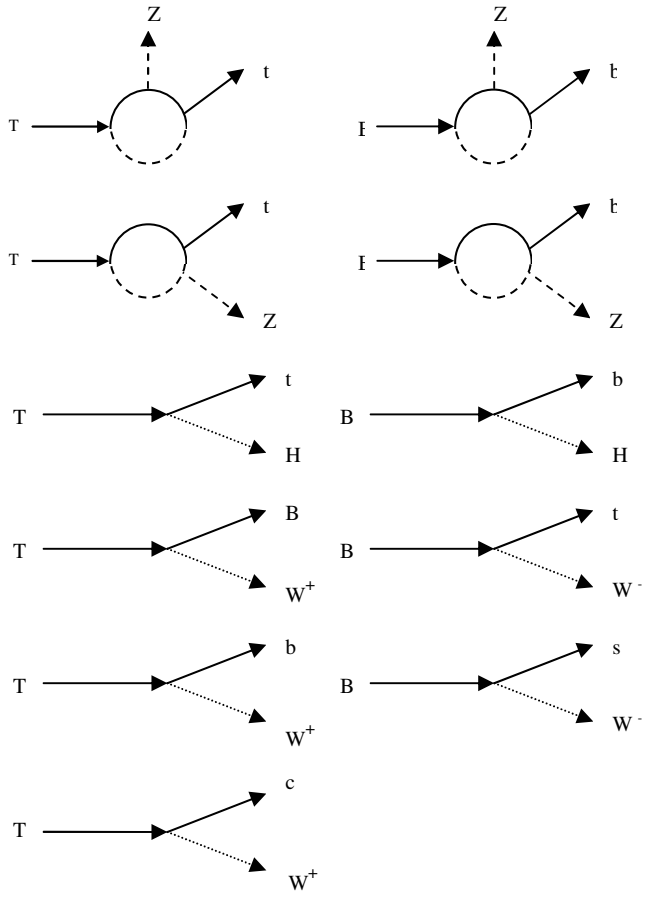

Figure 2. Presented here are the Feynman diagrams for the decays of both T and B quarks. Since here we are presuming that T is more massive than B there is one additional decay possibility for T ($T \rightarrow B + W^+$) than there is for B. The decays involving Z bosons are taken at one loop.

The decay rates involving real and virtual W bosons have already been calculated by Hou and Stuart [6], and their results are quoted below:

$$\Gamma_W\left(Q \rightarrow q + W^{\pm}\right) = 9\frac{{G_F}^2 {m_Q}^5}{192\pi^3} F\left[\left(\frac{m_Q}{m_W}\right)^2, \left(\frac{m_q}{m_Q}\right)^2\right]\left|V_{Qq}\right|^2, \tag{7}$$

$$F[\alpha,\beta] = 2\int_0^{\left(1-\sqrt{\beta}\right)^2} \frac{\left((1-\beta)^2 + (1+\beta)x - 2x^2\right)\sqrt{\left(1+\beta^2+x^2-2(\beta+\beta x+x)\right)}}{(1-x\alpha)^2 + \left(\frac{{\Gamma_W}^2}{{m_W}^2}\right)} dx\,. \tag{8}$$

The function F is a three body phase factor whose arguments α and β are defined in the decay rate involving the W boson. The variable x specifies where in phase space we are and the integration over x takes into account all possible phase space contributions. G_F is the Fermi constant, V_{Qq} is the CKM mixing matrix element for interactions between Q and q which we have taken to be $V_{Qq} = \sqrt{\frac{m_q}{m_Q}}$, where m_Q and m_q denote the initial and daughter quark masses, m_W is the mass of the W boson, and Γ_W is the decay width of the W boson. The validity of this equation has been independently confirmed by us. The decay width for Z decays was calculated by Frampton and Hung [1] for the chiral case at one loop and is quoted below for both T and B quarks.

$$\lambda[x, y, z] = x^2 + y^2 + z^2 - 2xy - 2yz - 2xz, \tag{9}$$

$$P[i, j] = \sqrt{\lambda\left[1, \left(\frac{m_Z}{i}\right)^2, \left(\frac{j}{i}\right)^2\right]}\left(\left(1 - \left(\frac{j}{i}\right)^2\right)^2 + \left(\frac{m_Z}{i}\right)^2\left(1 + \left(\frac{j}{i}\right)^2\right) - 2\left(\frac{m_Z}{i}\right)^4\right), \tag{10}$$

the two body phase space factor,

$$\Delta[i, j] = \left(\left(\frac{i^2 - j^2}{{m_W}^2}\right)\left(Log\left[\frac{{m_W}^2}{i^2}\right] - 1\right)\right)^2, \tag{11}$$

a function describing the presence of the loop in decays involving Z bosons in Figure 2,

$$\Gamma(T \to t + Z) = \frac{G_F {m_T}^3}{4\pi\sqrt{2}Cos[\theta_W]^2}\left(\left(\frac{g^2}{16\pi^2}\right)\Delta[m_B, m_b]\right)P[m_T, m_t]\,|V_{bT}|^2, \tag{12}$$

$$\Gamma(B \to b + Z) = \frac{G_F {m_B}^3}{4\pi\sqrt{2}Cos[\theta_W]^2}\left(\left(\frac{g^2}{16\pi^2}\right)\Delta[m_T, m_t]\right)P[m_B, m_b]\,|V_{tB}|^2. \tag{13}$$

In these equations g is the electroweak coupling constant, θ_w is the electroweak mixing angle, m_Z is the mass of the Z boson, m_T is the fourth generation top quark mass, m_B is the

fourth generation bottom quark mass, m_t is the top quark mass, and m_b is the top quark mass. The decay widths for $T \rightarrow t+H$ and $B \rightarrow b+H$ were calculated by Professor Sher and I for the two body case [3]. The differential formula for the decay width is [7]

$$d\Gamma = \frac{1}{32\pi^2} |M|^2 \frac{|\mathbf{p}_q|}{m_Q{}^2} d\Omega . \tag{14}$$

Here M is the invariant amplitude for the decay process, m_Q is the mass of the heavy decaying quark, $\mathbf{p}_q$ is the momentum of the daughter quark, and $d\Omega = d\varphi_q d(\cos\theta_q)$ is the solid angle of the daughter quark. The invariant amplitude M for a decay process involving a scalar particle is given by

$$M = g_H \, \bar{u}(p_q) u(p_Q), \tag{15}$$

which is angle independent. Here $\bar{u}(p_q)$ and $u(p_Q)$ are the Dirac spinors for initial and final particles respectively. Evaluation of the modulus squared of M using well known trace theorems yields [3]:

$$|M|^2 = 4 g_H{}^2 m_Q (E_q + m_q). \tag{16}$$

While the values of E_q and $\mathbf{p}_q$ are

$$|\mathbf{p}_q| = \frac{\left(\left(m_Q{}^2 - (m_q + m_H)^2 \right) \left(m_Q{}^2 - (m_q - m_H)^2 \right) \right)^{\frac{1}{2}}}{2m_Q}, \tag{17}$$

$$E_q = \frac{m_Q{}^2 - m_H{}^2 + m_q{}^2}{2m_Q}. \tag{18}$$

None of these values have an angular dependence, so we may immediately integrate over the solid angle element, adding a factor of 4π to our expression. Our final expression for the $Q \rightarrow q+H$ decay rate is

$$\Gamma_H(Q\to q+H)=g_H{}^2\frac{m_Q}{8\pi}\left(1-\frac{m_H{}^2-m_q{}^2-2m_qm_Q}{m_Q{}^2}\right)\sqrt{\left(1-\left(\frac{m_q}{m_Q}+\frac{m_H}{m_Q}\right)^2\right)\left(1-\left(\frac{m_q}{m_Q}-\frac{m_H}{m_Q}\right)^2\right)}. \quad (19)$$

Here m_H is the mass of the Higgs particle. It is in the Higgs decay width where the type III ansatz is incorporated as described in the work by Cheng and Sher [5], giving the following coupling constant:

$$g_H=\frac{\sqrt{m_Qm_q}}{175GeV}. \quad (20)$$

Using these equations for the decay widths, plots of the branching ratios were created using Mathematica. Due to the complexity of the integration in equation 6, the numerical integration function of Mathematica had to be used. A branching ratio for a particular decay process is the ratio of that decay width to the sum of all decay widths. Choice of the Higgs mass was motivated by experimental bounds. The Higgs masses considered here are 130 GeV, 150 GeV, and 200 GeV. The masses of the *T* and *B* quarks were more difficult to decide upon. Two schemes were devised. In the first, the *T* mass was defined as 1.1 times that of the *B* mass. The motivation for this relation comes from the value of the ρ parameter constraint: $m_T/m_B<1.1$ [1]. In the second, the *T* mass was 440 GeV and the *B* mass was allowed to vary or the *B* mass was 400 and the *T* mass was allowed to vary. The choice of different constant masses for *T* and *B* is again due to the ρ parameter constraint. The color scheme for the *T* decays is as follows: $T\to t+Z$ in red, $T\to t+H$ in green, $T\to B+W^+$ in blue, $T\to b+W^+$ in purple, and $T\to c+W^+$ in black. The scheme for the *B* decays was $B\to b+Z$ in red, $B\to b+H$ in green, $B\to t+W^-$ in blue, and $B\to s+W^-$ in black. The results are presented on the following semi-log plots.

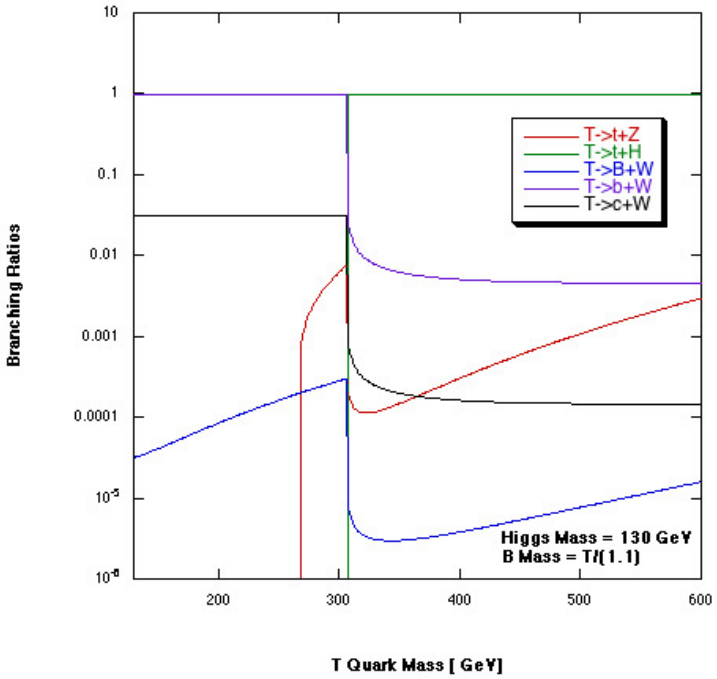

Figure 3. *T* quark branching ratios with Higgs mass of 130 GeV. The mass scheme in place is $m_B=m_T/1.1$. The ratios are color coded in the following manner: $T\rightarrow t+Z$ in red, $T\rightarrow t+H$ in green, $T\rightarrow B+W^+$ in blue, $T\rightarrow b+W^+$ in purple, and $T\rightarrow c+W^+$ in black. Notice the dominance of the $T\rightarrow t+H$ decay channel.

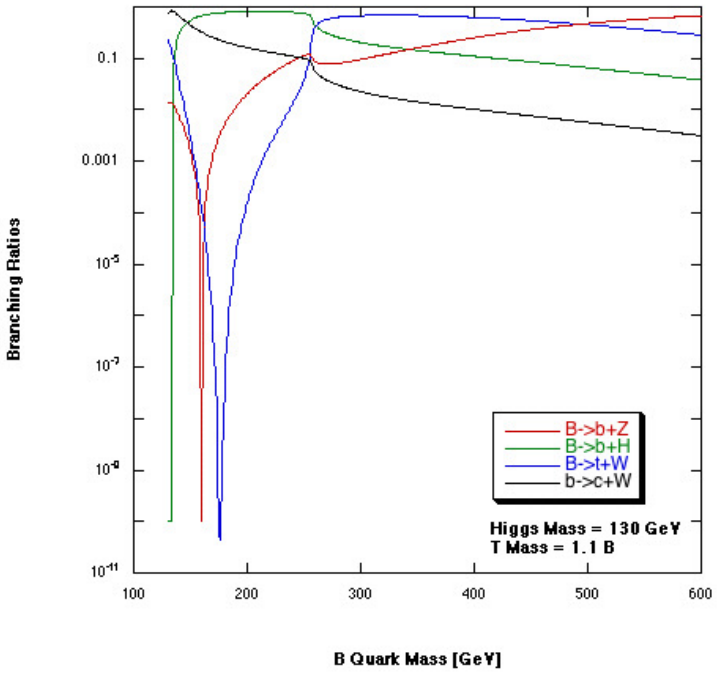

Figure 4. *B* quark branching ratios with a Higgs mass of 130 GeV. The mass scheme in place is $m_T=1.1\ m_B$. The ratios are color coded in the following manner: $B\rightarrow b+Z$ in red, $B\rightarrow b+H$ in green, $B\rightarrow t+W^-$ in blue, and $B\rightarrow s+W^-$ in black. Notice the heavy dependence upon *B* quark mass.

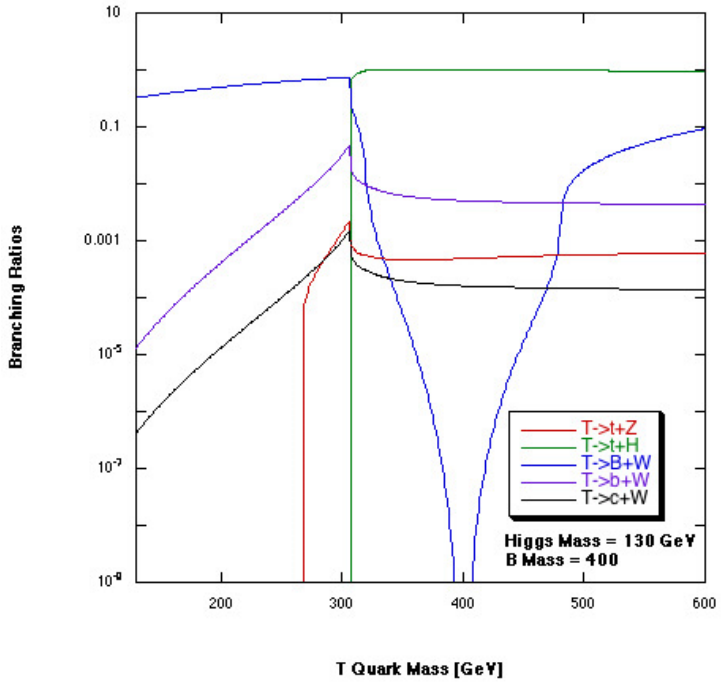

Figure 5. *T* quark branching ratios with Higgs mass of 130 GeV. The mass scheme in place is m_B= 400 GeV with varying *T* quark mass. The ratios are color coded in the following manner: $T \rightarrow t+Z$ in red, $T \rightarrow t+H$ in green, $T \rightarrow B+W^+$ in blue, $T \rightarrow b+W^+$ in purple, and $T \rightarrow c+W^+$ in black. Notice the dominance of the $T \rightarrow t+H$ decay channel.

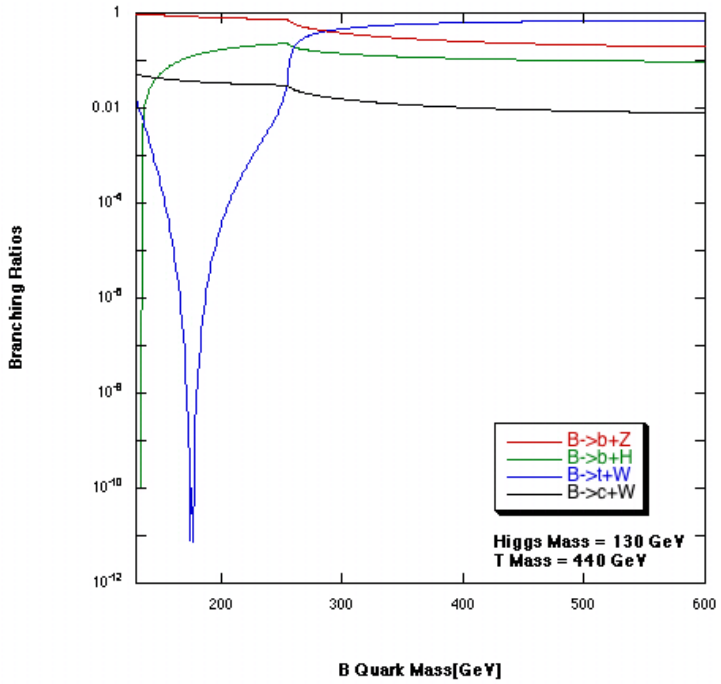

Figure 6. *B* quark branching ratios with a Higgs mass of 130 GeV. The mass scheme in place is m_T =440 GeV and with varying B quark mass. The ratios are color coded in the following manner: $B \rightarrow b+Z$ in red, $B \rightarrow b+H$ in green, $B \rightarrow t+W^-$ in blue, and $B \rightarrow s+W^-$ in black. Notice the heavy dependence upon *B* quark mass.

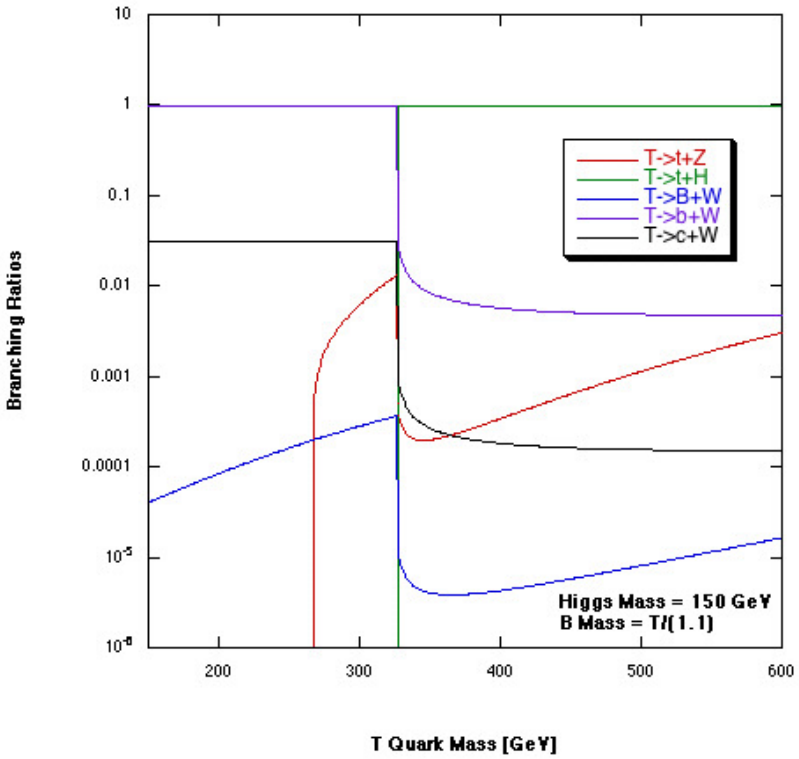

Figure 7. *T* quark branching ratios with Higgs mass of 150 GeV. The mass scheme in place is $m_B=m_T/1.1$. See Figure 3 caption.

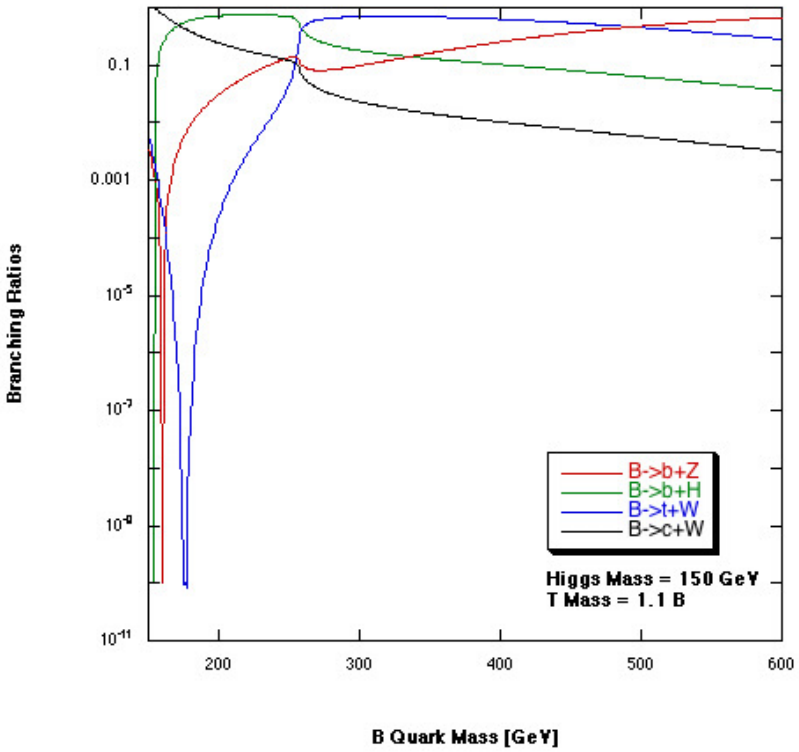

Figure 8. *B* quark branching ratios with a Higgs mass of 150 GeV. The mass scheme in place is $m_T=1.1\ m_B$. See Figure 4 caption.

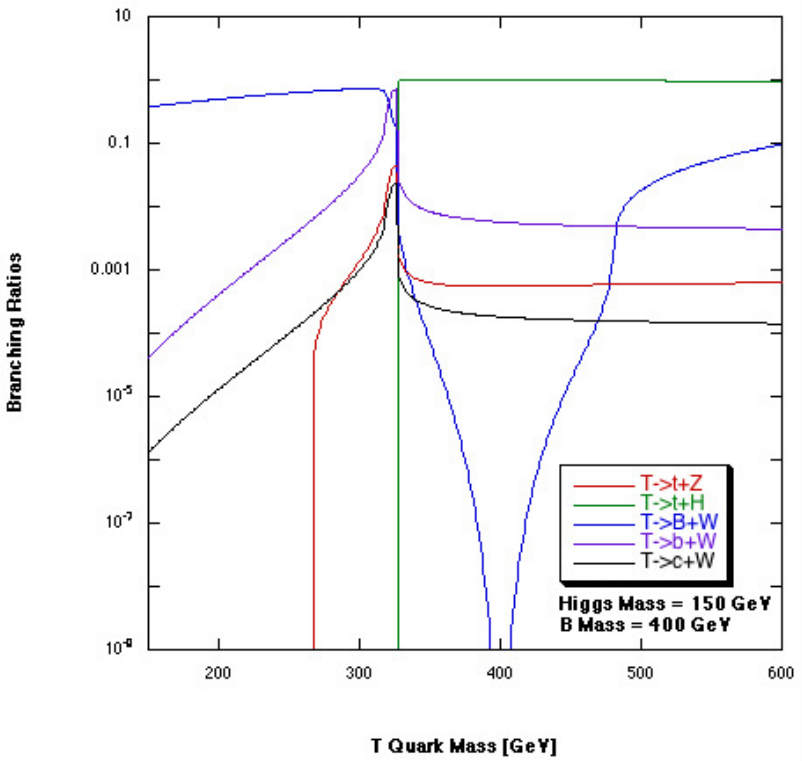

Figure 9. *T* quark branching ratios with Higgs mass of 150 GeV. The mass scheme in place is m_B= 400 GeV with varying *T* quark mass. See Figure 5 caption.

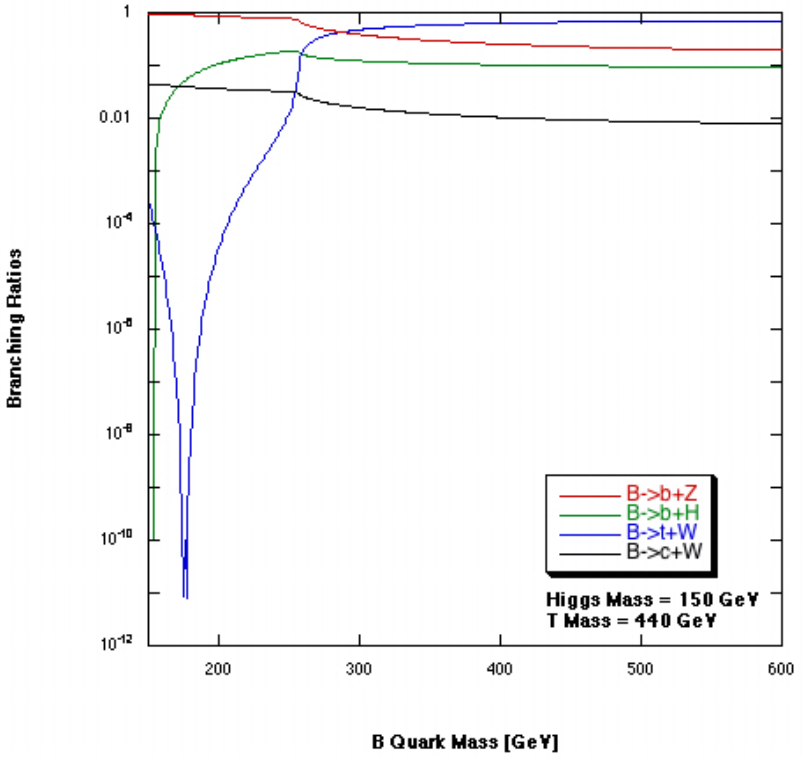

Figure 10. *B* quark branching ratios with a Higgs mass of 150 GeV. The mass scheme in place is m_T =440 GeV and with varying B quark mass. See Figure 6 caption.

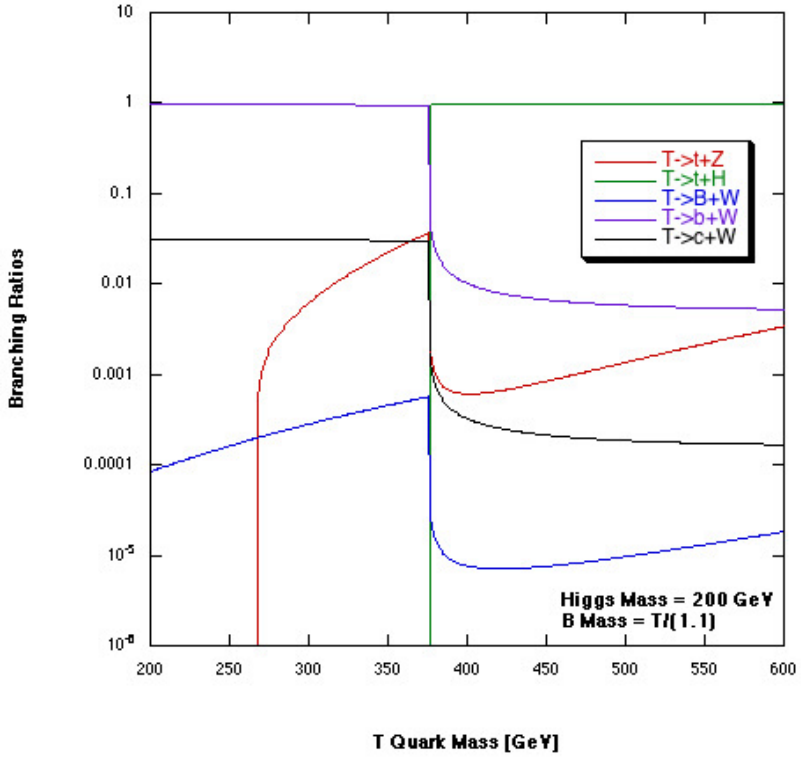

Figure 11. *T* quark branching ratios with Higgs mass of 200 GeV. The mass scheme in place is $m_B=m_T/1.1$. See Figure 3 caption.

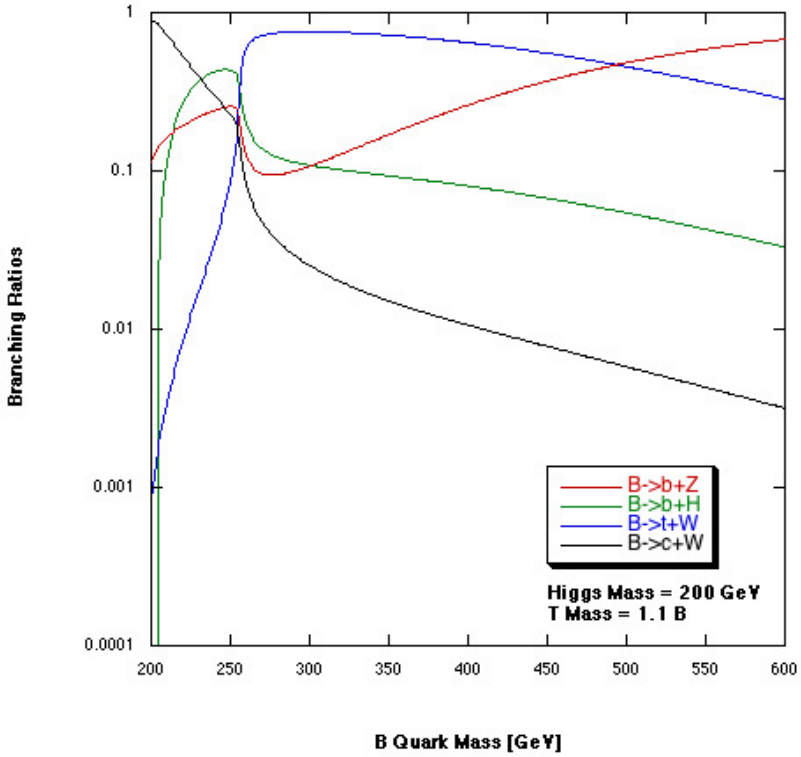

Figure 12. *B* quark branching ratios with a Higgs mass of 200 GeV. The mass scheme in place is $m_T=1.1\ m_B$. See Figure 4 caption.

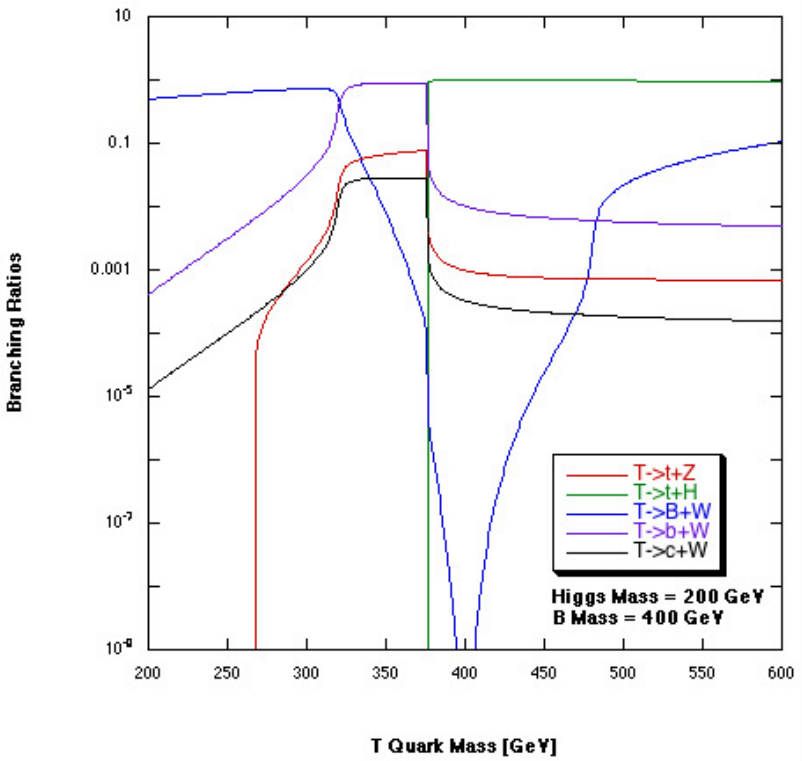

Figure 13. *T* quark branching ratios with Higgs mass of 200 GeV. The mass scheme in place is m_B= 400 GeV with varying *T* quark mass. See Figure 5 caption.

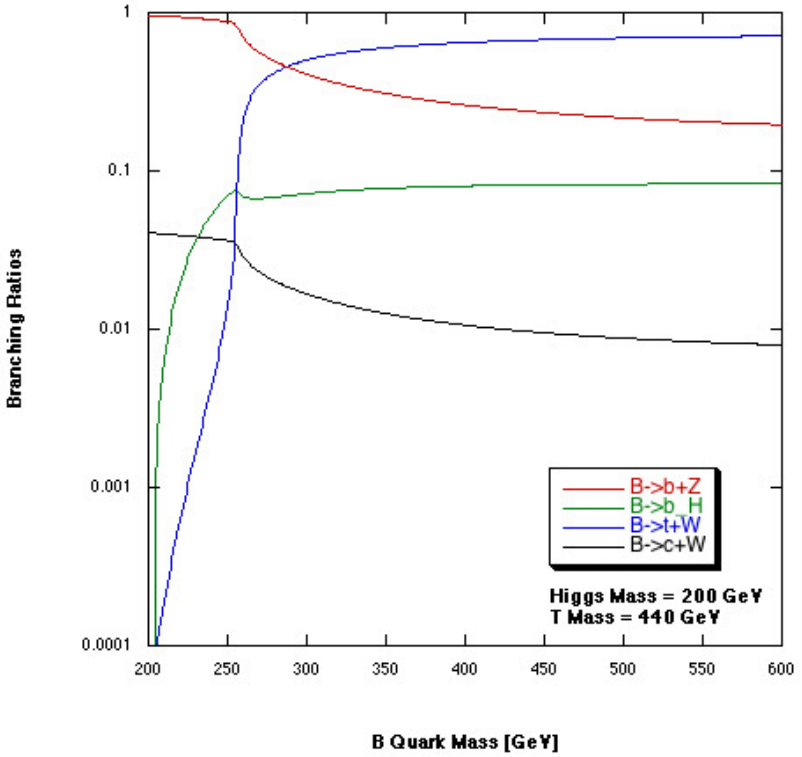

Figure 14. *B* quark branching ratios with a Higgs mass of 200 GeV. The mass scheme in place is m_T =440 GeV and with varying B quark mass. See Figure 6 caption.

These plots illustrate the complex phenomenology of fourth generation decays. In particular B quark decays are surprisingly dependent upon the mass of the Higgs boson as well as T quark mass. Despite the varying characteristic of these decays, one overarching principle holds for the T quark decays: the $T \rightarrow t+H$ channel dominates overwhelmingly over all other channels. Indeed provided that this decay channel is accessible, the branching ratio is very close to one for all T mass schemes and Higgs masses examined. Thus, if the 2HDM type III is a valid description of new physics and if the fourth generation is a reality, the $T \rightarrow t+H$ channel will completely dominate. A signal from this decay can potentially demonstrate the existence of both the Higgs boson and a fourth generation of fermions, an unequivocal signature of physics beyond the Standard Model.

3. Detection at the Large Hadron Collider

As demonstrated in the previous section, in the 2HDM type III with a fourth generation the $T \rightarrow t+H$ decay overwhelmingly dominates T quark decay processes. The only prospect for the detection of these particles is the Large Hadron Collider, a proton-proton collider nearing completion at CERN in Geneva, Switzerland. The proton beams collide with an energy of 7 TeV each, a dramatic improvement over previous accelerators [8]. We will now investigate possibilities for detection at the LHC when it begins operation in November, 2007.

3.1 Computing the Reaction Cross Section

3.1.1 Subprocess Cross Section

Computing the cross sections for a hadron-hadron collider is a relatively elementary calculation. The first consideration is determining the relevant subprocesses for the reaction. The reaction process under examination is,

$$PP \rightarrow T\overline{T} \rightarrow t\bar{t}HH\,, \tag{21}$$

where P designates a proton, T and t designate fourth and third generation top quarks respectively, a bar denotes an antiparticle, and H is the lightest neutral Higgs boson in the 2HDM type III. There are a variety of subprocesses in this interaction which produce heavy quarks. The two dominating subprocesses are

$$PP \rightarrow q\overline{q} \rightarrow T\overline{T}\,, \tag{22}$$

$$PP \rightarrow gg \rightarrow T\overline{T}\,. \tag{23}$$

Here q represents a quark and g represents a gluon. To obtain the total cross section, we must first determine the cross sections for these two subprocesses. The differential cross

sections for these processes can easily be found in a standard treatment of hadroproduction [4]:

$$\frac{d\hat{\sigma}}{d\hat{t}}(q\bar{q}\to Q\bar{Q})=\frac{4\pi\alpha_s^{\,2}}{9\hat{s}^4}\left[\left(m^2-\hat{t}\right)^2+\left(m^2-\hat{u}\right)^2+2m^2\hat{s}\right]\left[\left(1-\frac{4m^2}{\hat{s}}\right)^{\frac{1}{2}}\left(1+\frac{2m^2}{\hat{s}}\right)\right] \quad (24)$$

$$\frac{d\hat{\sigma}}{d\hat{t}}(gg\to Q\bar{Q})=\frac{\pi\alpha_s^2}{8\hat{s}^2}\left[\begin{array}{l}\frac{6\left(m^2-\hat{t}\right)^2\left(m^2-\hat{u}\right)^2}{\hat{s}^2}-\frac{m^2\left(\hat{s}-4m^2\right)}{3\left(m^2-\hat{t}\right)\left(m^2-\hat{u}\right)}+\\ \frac{4}{3}\frac{\left(m^2-\hat{t}\right)\left(m^2-\hat{u}\right)-2m^2\left(m^2+\hat{t}\right)}{\left(m^2-\hat{t}\right)^2}+\frac{4}{3}\frac{\left(m^2-\hat{t}\right)\left(m^2-\hat{u}\right)-2m^2\left(m^2+\hat{u}\right)}{\left(m^2-\hat{u}\right)^2}\\ -3\frac{\left(m^2-\hat{t}\right)\left(m^2-\hat{u}\right)+m^2\left(\hat{u}-\hat{t}\right)}{\hat{s}\left(m^2-\hat{t}\right)}-3\frac{\left(m^2-\hat{t}\right)\left(m^2-\hat{u}\right)+m^2\left(\hat{t}-\hat{u}\right)}{\hat{s}\left(m^2-\hat{u}\right)}\end{array}\right]\left[\left(1-\frac{4m^2}{\hat{s}}\right)^{\frac{1}{2}}\left(1+\frac{2m^2}{\hat{s}}\right)\right] \quad (25)$$

Where α_s is the strong coupling constant, and the invariant kinematic variables for an interaction A + B → C + D are defined to be [3]

$$\begin{aligned}\hat{s}&=\left(p_A+p_B\right)^2,\\ \hat{t}&=\left(p_A-p_C\right)^2,\\ \hat{u}&=\left(p_A-p_D\right)^2,\\ \hat{s}&\propto s=(2\times 7TeV)^2.\end{aligned} \quad (26)$$

The ^ notation signifies that these variables are for the subprocess rather than the entire production reaction. Here s is two times the proton beam energy of 7 TeV squared and p_i represents a particle's four momentum. There is a useful relation between these variables and the center of mass scattering angle [4].

$$\begin{aligned}\hat{t}&=-\frac{1}{2}\hat{s}\left(1-\cos\theta\right)\\ \hat{u}&=-\frac{1}{2}\hat{s}\left(1+\cos\theta\right)\end{aligned} \quad (27)$$

Upon substituting these into our equations for the subprocess differential cross sections we can obtain the cross sections themselves:

$$d\hat{t} = \frac{1}{2}\hat{s}d(\cos\theta)$$
$$\Rightarrow \hat{\sigma}_{q\bar{q}} = \int \frac{d\hat{\sigma}_{q\bar{q}}}{d\hat{t}} d\hat{t} = \int_{-1}^{1} \frac{d\hat{\sigma}_{q\bar{q}}}{d\hat{t}} \left(\frac{1}{2}\hat{s}\right) d(\cos\theta) \tag{28}$$
$$\Rightarrow \hat{\sigma}_{gg} = \int \frac{d\hat{\sigma}_{gg}}{d\hat{t}} d\hat{t} = \int_{-1}^{1} \frac{d\hat{\sigma}_{gg}}{d\hat{t}} \left(\frac{1}{2}\hat{s}\right) d(\cos\theta)$$

which become

$$\hat{\sigma}_{q\bar{q}} = \frac{8\pi\alpha_s{}^2}{27\hat{s}^3}\left(3m^4 + 6m^2\hat{s} + \hat{s}^2\right)\left(1 - \frac{4m^2}{\hat{s}}\right)^{\frac{1}{2}}\left(1 + \frac{2m^2}{\hat{s}}\right), \tag{29}$$

$$\hat{\sigma}_{gg} = \frac{\left(\begin{array}{l}\pi\alpha_s{}^2\left(2m^2 + \hat{s}\right)\left(9m^6 - 9m^4\hat{s} - 41m^2\hat{s}^2 - 7\hat{s}^3\right) + \\ 8\left(m^2 + \hat{s}\right)\left(3m^2 + \hat{s}\right)\left(3m^4 + 5m^2\hat{s} + \hat{s}^2\right)\operatorname{arctanh}\left(\frac{\hat{s}}{2m^2 + \hat{s}}\right)\end{array}\right)}{12\hat{s}^3\left(m^2 + \hat{s}\right)\left(2m^2 + \hat{s}\right)}\left(1 - \frac{4m^2}{\hat{s}}\right)^{\frac{1}{2}}\left(1 + \frac{2m^2}{\hat{s}}\right). \tag{30}$$

The running strong coupling constant, α_s, is taken as 0.1 at this energy scale and m is the T quark mass. Now that the subprocess cross sections have been obtained, the total production cross section can be determined.

3.1.2 Total Production Cross Section

Our final goal is to determine the total production cross section for the $PP \to T\bar{T}$ process. This will enable us to determine how frequently T quarks are produced at the LHC. We have already determined the subprocess cross sections for heavy quark production via quark anti quark collisions and gluon-gluon fusion in equations 29 and 30. In particular, we want to examine fourth generation top quark production. The formula for the total cross section is

$$\sigma\left(PP \to T\bar{T}\right) = \sum_{a,b} C_{ab} \int_{\frac{4m^2}{s}}^{1} d\tau \int_{\tau}^{1} dx \frac{1}{x}\left(f_a(x) f_b\left(\frac{\tau}{x}\right) + \left(A \leftrightarrow B \, if \; a \neq b\right)\right)\hat{\sigma}_{ab}(\hat{s} = \tau s). \tag{31}$$

where C_{ab} are the initial color averaging factors for quarks and gluons, $f_i(x)$ are the parton distribution functions, $\sqrt{s}$ is two times the proton beam energy (7 TeV). The lower limit of the integral over τ is set by phase space restrictions, below which the parton distribution functions become unreliable. A sum is performed over all possible subprocesses under consideration: $\left(gg, u\bar{u}, \bar{u}u, d\bar{d}, \bar{d}d\right) \to T\bar{T}$. The color averaging factors for these processes are $C_{q\bar{q}} = \frac{1}{9}$ for quark anti quark interactions and $C_{gg} = \frac{1}{64}$ for the gluon fusion case. The most important functions in this equation are the parton distribution functions for the proton, $f_i(x)$ [4]. The proton is composed of two up quarks and one down quark, however these quarks add up to about 16 MeV, while the mass of the proton is approximately 938 MeV [7]. This missing mass is hidden in the energy of the gluons mediating the strong force within the proton. This energy can result in the production of virtual gluons and quarks distributed within the proton. The two up and one down quark observed are called the valence quarks. The parton distribution functions, determined experimentally, govern how likely it is that a particular virtual particle is present within the proton [4]. We used the CTEQ 6 distribution functions, which have the following general formulation [9]:

$$xf(x,Q_0) = A_0 x^{A_1} (1-x)^{A_2} e^{A_3 x} \left(1 + e^{A_4 x}\right)^{A_5}, \tag{32}$$

$$xf(x,Q_0) = A_0 x^{A_1} (1-x)^{A_2} + (1 + A_3 x)(1-x)^{A_4}, for\left(\frac{\bar{d}}{\bar{u}}\right). \tag{33}$$

The coefficients are given in Table 1 [9].

	A_0	A_1	A_2	A_3	A_4	A_5
d_v	1.4473	0.6160	4.9670	−0.8408	0.4031	3.0000
u_v	1.7199	0.5526	2.9009	−2.3502	1.6123	1.5917
g	30.4571	0.5100	2.3823	4.3945	2.3550	−3.0000
$\bar{u}+\bar{d}$	0.0616	−0.2990	7.7170	−0.5283	4.7539	0.6137
$s=\bar{s}$	0.0123	−0.2990	7.7170	−0.5283	4.7539	0.6317
$\bar{d}/\bar{u}$	33657.8	4.2767	14.8586	17.000	8.6408	−

Table 1. CTEQ 6 parton distribution function coefficients for up and down valence quarks, gluons, the sum of anti up and down quarks, strange and anti strange quarks, and the ratio of anti down quarks to anti up quarks.

Simple manipulations give the distributions for up and down quarks, gluons, and their respective antiparticles. Now that we have the distributions, we can calculate the total cross section as a function of *T* quark mass. There are five relevant subprocesses:

$$\left(gg, u\bar{u}, \bar{u}u, d\bar{d}, \bar{d}d\right) \rightarrow T\bar{T} \tag{34}$$

We used Mathematica's numerical integration function to compute the results, presented in figure 15 in picobarns (pb). Note that 1 GeV^{-2} =389 x 10^{-6} barns.

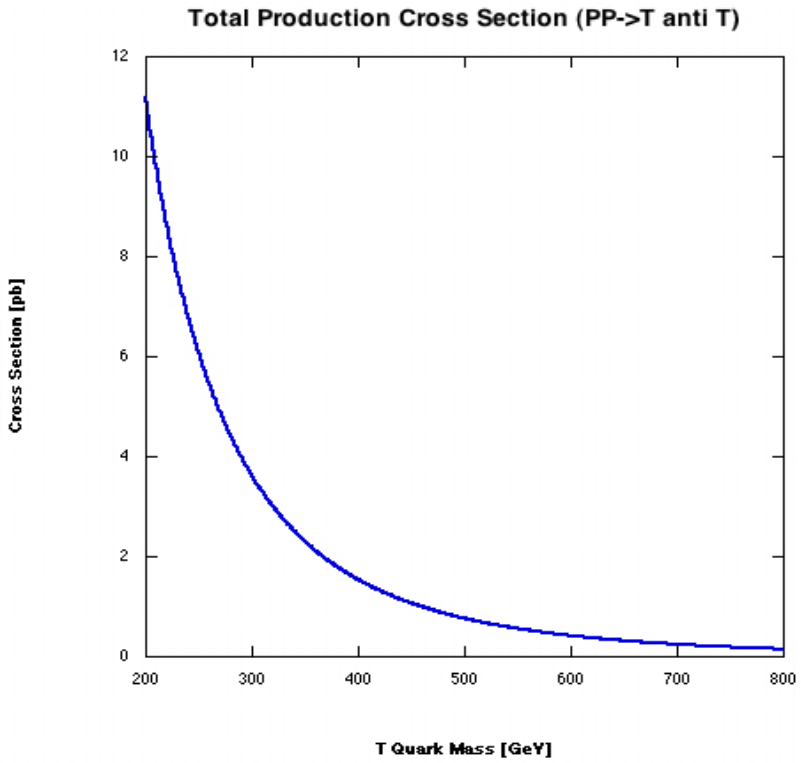

Figure 15. Total production cross section presented in picobarns (pb) as a function of *T* quark mass (GeV). The LHC beam energy is assumed to be 7 TeV per beam (14 TeV total). The steep drop off of the cross section shows that fourth generation production is heavily dependent on the mass of the *T* quark.

With the total cross section for fourth generation top quark production, we can now delve into how many $T \rightarrow t+H$ decays will be observed and examine possible signals of new physics.

3.2 Prospects for Detection

3.2.1 Expected Events per Day

The Large Hadron Collider has sufficient energy to produce physics beyond the Standard Model prescription. The question relevant to this thesis concerns how many $T \rightarrow t+H$ events should be expected. Computing the number follows a simple formulation where the number of events is equal to the product of the total production cross section, LHC beam luminosity, and the branching ratio of the $T \rightarrow t+H$ decay channel. The total

production cross section was calculated in the previous section. The LHC beam luminosity was obtained from the *LHC Design Report vol 1* and has a value of 10^{34} cm^{-2} s^{-1} [10]. The branching ratio for this channel was obtained in section 2.3 of this thesis. These results are all a function of *T* and *H* masses. The branching ratio for this process is only valid in the two body $T \rightarrow t+H$ regime since we only have its branching ratio for the two body case, placing a restriction on what we can choose our particle masses to be. In particular, $m_T - m_H \geq m_t \approx 176 GeV$. With this restriction in place, we can begin to explore *T* production.

T mass (GeV)	*H mass (GeV)*	*Events per day*
440	130	694
440	150	694
440	200	692
520	130	399
520	150	399
520	200	398
600	130	242
600	150	242
600	200	242

Table 2. Fourth generation production events per day as a function of various *H* and *T* masses. The *B* quark mass does affect the $T \rightarrow t+H$ branching ratio and is assumed to be $m_T/1.1$ for simplicity. No significant dependence upon Higgs mass is expected, since the dominance of the $T \rightarrow t+H$ is unaffected by Higgs mass.

Results for various *T* quark masses and Higgs masses are shown in Table 2. *B* quark mass was taken as $m_T/1.1$ for simplicity. There is no significant correlation between the number of $PP \rightarrow T\overline{T}$ events and Higgs mass as expected: the dominance of the $T \rightarrow t+H$ decay did not depend upon Higgs mass. There is however a significant dependence upon *T* quark mass, as we expect from the production cross section in Figure 15.

3.2.2 Characterization of the $T \rightarrow t+H$ Decay Channel

In this section we will examine the details of the $T \rightarrow t+H$ decay channel. Whenever a fourth generation top event occurs, an anti top quark is also produced. The decay formulas for the anti particle are identical to those for the fourth generation top. Since each decay results in production of a Higgs particle, the net result is the production of two Higgs bosons per event. A diagram of this process is shown in figure 16.

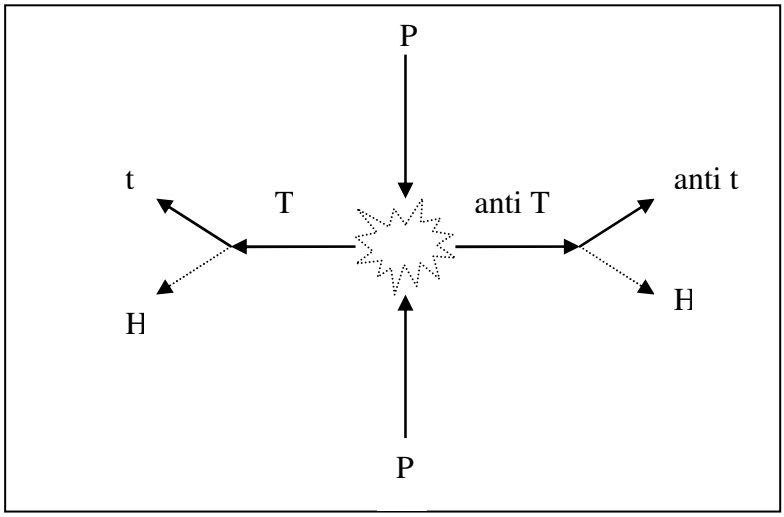

Figure 16. Diagram of a proton-proton collision giving rise to the production of a T quark and its anti particle. These quarks subsequently decay via the dominant decay channel, $T \rightarrow t+H$.

The branching ratios for a standard model Higgs particle, were used for our 2HDM type III Higgs particle [11]. While not identical, they are sufficient for our purposes here. The ratios are presented in Table 3.

Higgs mass (GeV)	H→bb	H→ττ	H→μμ	H→ss	H→cc	H→tt
130	0.5271	5.41×10^{-2}	1.88×10^{-4}	3.92×10^{-4}	2.40×10^{-2}	0
150	0.1757	1.85×10^{-2}	6.42×10^{-5}	1.31×10^{-4}	7.98×10^{-3}	0
200	2.599 X 10-3	2.887×10^{-4}	1×10^{-5}	1.93×10^{-6}	1.18×10^{-4}	0

Higgs mass (GeV)	H→gg	H→γγ	H→Zγ	H→WW	H→ZZ	H→tt
130	6.48×10^{-2}	2.23×10^{-3}	1.93×10^{-3}	0.2869	3.84 X 10-02	0
150	2.93×10^{-2}	1.39×10^{-3}	2.39×10^{-3}	0.6817	8.28 X 10-02	0
200	8.25×10^{-4}	5.25×10^{-5}	1.77×10^{-4}	0.7347	0.2613	0

Table 3. Branching ratios for a SM Higgs boson taken from [11].

An examination shows that the most significant decay modes at these masses are the ZZ, WW, and $b\bar{b}$ modes. ZZ, WW, and $b\bar{b}$ pair production from Higgs pairs is presented in Table 4. Also included in Table 4 is the number of Higgs pairs produced by competing processes, inferred from Figure 7 in [12] for a Higgs mass of 200 GeV. The total Standard Model pair production with QCD corrections was calculated by Dawson et al. and pales in comparison to what has been demonstrated here.

Higgs mass (GeV)	T mass (GeV)	Events per day	Higgs pairs per day	SM Higgs pairs per day	4 W events per day	4 Z events per day	2 $b\bar{b}$ events per day
130	440	694	694	*No estimate made.*	114	~2	386
	520	399	399		66	~1	222
	600	242	242		30	~1	134
150	440	694	694		645	10	43
	520	399	399		371	6	25
	600	242	242		225	3	15
200	440	692	692	22	747	95	0
	520	398	398		430	54	0
	600	242	242		261	33	0

Table 4. Decay phenomenology of the Higgs boson. Fourth generation *T* events per day, fourth generation Higgs pair production per day, SM Higgs pair production per day [12], number of *H* pairs decaying to four W bosons, four Z bosons, or to two $b\bar{b}$ pairs are all displayed in this table.

At low Higgs mass, 130 and 150 GeV, $b\bar{b}$ pair production dominates over the production of four W or Z bosons. However b quarks are difficult to detect at the LHC due to significant QCD backgrounds, which necessitates delicate kinematic cuts for any realistic hope of detection [13,14]. At higher mass, 200 GeV, the $b\bar{b}$ quark production shuts off entirely, switching over to the WW and ZZ boson decay channels. Although *H* decay at this mass primarily goes to W bosons rather than Z bosons, it is more interesting to examine the phenomenology of the Z bosons. If each of the four Z bosons decays into a pair of first or second generation leptons (third generation particles decay too quickly), then we have an eight lepton "gold plated" signal. This signal has essentially no

background since Higgs pair production by other means is smaller by a factor of 10 than that achieved via *T* decays, making it an unequivocal signature of new physics.

Determining the probability of an eight lepton signal was undertaken in the following manner. The branching ratio for Z decay to an electron and a positron or a muon and an anti muon is 0.0336, given by the Particle Data Group [7]. The probability for both ZZ pairs to go to electron positron or muon anti muon pairs is 1.27455×10^{-6}. However, it is important to consider all decay possibilities. For instance, one Z pair could decay to electron positron pairs while the other pair could go to muon anti muon pairs. Counting up these possibilities gives 16 total eight lepton decays, which increases our probability of all four Z particles decaying to lepton pairs to 2.0393×10^{-5}. The number of events per year for various *T* and *H* masses are shown in Table 5.

	Higgs mass 130 GeV	Higgs mass 150 GeV	Higgs mass 200 GeV
T mass (GeV)	Number of eight lepton events per year		
440	0.061	0.283	2.81
520	0.035	0.162	1.62
600	0.021	0.099	0.98

Table 5. Number of eight lepton events per year as a function of *T* quark and *H* boson mass.

For low Higgs masses we see no eight lepton events. However for the 200 GeV Higgs mass we will have one to four events per year, depending upon *T* quark mass. With no competing processes, detection of this eight lepton signal would be an undeniable confirmation of the 2HDM type III and the fourth generation, even if detectors only resolved it once per year.

	Higgs mass 130 GeV	Higgs mass 150 GeV	Higgs mass 200 GeV
T mass (GeV)	Number of four lepton events per year		
440	176	379	1192
520	101	218	686
600	61	132	417

Table 6. Number of silver plated events per year as a function of *T* quark and *H* boson mass.

Another prospect for detection is the observation of a four lepton "silver plated" signal. In this case only one of our two Higgs particles decays to a pair of Z bosons and subsequently into a set of four leptons. While this is not as conclusive a signature as a true gold plated event, it may be detectable at the LHC. As shown in Table 6, four lepton decays occur far more frequently than eight lepton decays regardless of Higgs mass. However high production does not guarantee detection of a four lepton mode; background processes for this mode arise from single Higgs production at the LHC. The processes that can give rise to a single Higgs are numerous, and an excellent treatment of the next to next to leading order total single Higgs production cross section can be found in [15]. The total cross section for single Higgs production was inferred from Figure 1 in [15] and is 10 to 100 times greater than our total production cross section, which was on the order of 1 pb (see Figure 15). This level of production will complicate detection of four lepton decays, however it will not preclude it. Four lepton events differ from single Higgs production in that each four lepton event is accompanied by a sister Higgs particle decaying into various QCD jets. These jets may be identified and used to differentiate four lepton events from single Higgs production backgrounds. Detection via this four lepton mode is not significantly more difficult than the eight lepton mode. Combined

with its extremely high production rate, both four and eight lepton events must be pursued in searches for the fourth generation and Higgs boson.

4. Conclusion

This thesis has been an examination of the phenomenology of a fourth generation of quarks in the context of the 2HDM type III. We have shown that with reasonable assumptions on the nature of the fourth generation as well as mass of the Higgs particle, it is possible to use the signals from an eight lepton (gold plated) event and a four lepton (silver plated) event to infer the presence of new physics at the LHC. Four lepton signals can be extracted from the data despite the high background generated by single Higgs production. Furthermore, although the eight lepton signals will occur at best four times per year, the nonexistent background makes detection of these events relatively easy. Both four and eight lepton signals are vital decay channels to include in searches at the LHC.

Future work on this topic should explore fourth generation detection prospects in the 2HDM type III over a wider range of particle masses and with higher order contributions. Understanding intricacies of the ATLAS detector at the LHC and what implications it has for four and eight lepton event detection prospects would also be an important issue to address. In the same vein, algorithms to extract four and eight lepton signals from ATLAS data should be devised and implemented. Finally, a deeper investigation into the phenomenology of the B quark and other fourth generation particles, as well as their interactions with SM particles, should be undertaken so that a more complete understanding of this hypothetical new sector can be achieved.

5. Acknowledgements

I would first like to thank Professor Marc Sher for his invaluable mentoring throughout the course of this project. I would also like to thank Professors Chris Carone, Gina Hoatson, and Leiba Rodman for serving on my committee. Lastly, but most certainly not least, I wish to thank my family and friends for their love and support.

References

[1] P.H. Frampton and P.Q. Hung, Phys. Rev. D **58**, 057704 (1998).

[2] P.H. Frampton, P.Q. Hung, and M. Sher, Physics Reports **330**, 263 (2000).

[3] F. Halzen and A.D. Martin, *Quarks and Leptons: An Introductory Course in Modern Particle Physics*. United States: John Wiley & Sons (1984).

[4] V.D. Barger and R.J.N. Philips (1997). *Collider Physics: Updated Edition*. United States: Addison-Wesley Publishing Company, Inc.

[5] T.P. Cheng and M. Sher, Phys. Rev. D **35**, p. 3383 (1987).

[6] W.S. Hou, R.G. Stuart, Phys. Rev. D **43**, p. 3669 (1991).

[7] J.D. Jackson. *The Review of Particle Physics: 38. Kinematics.* http://pdg.lbl.gov/2006/reviews/kinemarpp.pdf. United States: Particle Data Group (2006).

[8] J. Bagger et al., Phys. Rev. D **52**, p. 3878 (1995).

[9] J. Pumplin et al, CTEQ group, hep-ph/0201195.

[10] O. Bruning, P. Collier, P. Lebrun, S. Myers, R. Ostojic, J. Poole and P Proudlock, *LHC design report, vol. I. The LHC main ring,* CERN-2004-003.

[11] A. Djouadi, J. Kalinowski and M. Spira, Comp. Phys. Commun. 108 C (1998) 56, hep-ph/9704448.

[12] S. Dawson, S. Dittmaier and M. Spira, hep-ph/9805244.

[13] E. Arik et al., Phys.Rev.D **58**, 117701 (1998).

[14] J.L. Diaz–Cruz, H.–J. He, T. Tait, and C.–P. Yuan, Phys. Rev. Lett. 80 (1998) 4641.

[15] R.V. Harlander and W.B. Kilgore, Phys. Rev. Lett. 88 (2002) 201801, hep-ph/0201206.